Efficient removal of three dyes using porous covalent triazine frameworks: adsorption mechanism and role of pore distribution

Fengxia An, Jingliang Liu, Zhaoyi Xu and Shourong Zheng

ABSTRACT

Dyes are widely used in production and life. In this study, porous covalent triazine frameworks (CTFs) were synthesized and the adsorption behavior for three dyes was investigated by batch adsorption experiments. CTFs were characterized by various spectroscopic techniques for structure, porosity and surface properties. Several possible adsorption mechanisms were proposed including pore-filling, electrostatic attraction and hydrogen bonding interaction with the triazine structure of CTFs. The mechanisms were further verified by the pore size distribution and pH dependence. Additionally, CTF_{DCBP} displayed stronger adsorption affinity and faster adsorption kinetics for dyes, because of the wide pore size distribution. This study provides a new insight into the mesoporous CTFs, which exhibit great potential as an effective adsorbent for dye removal.

Key words | adsorption mechanism, covalent triazine framework, dyes, pore size

Fengxia An
State Power Environmental Protection Research Institute Co. Ltd,
Nanjing 210031,
China

Jingliang Liu (corresponding author)
School of Environmental Science,
Nanjing XiaoZhuang University,
Nanjing 211171,
China
E-mail: *jingliangliu@njxzc.edu.cn*

Zhaoyi Xu
Shourong Zheng
State Key Laboratory of Pollution Control and Resource Reuse, and School of the Environment,
Nanjing University,
Nanjing 210093,
China

HIGHLIGHTS

- Cation-π, hydrogen bond interaction and electrostatic interaction effect were responsible for strong adsorption of dyes to CTFs.
- Mesoporous CTF_{DCBP} shows dramatically enhanced adsorption and fast adsorption kinetics for large dyes Chrysophenine G due to the wide pore size distribution, homogeneous and regular-shaped structure.

INTRODUCTION

Dyes are widely used in various fields, including textile, leather, paper, plating, medicine and food industries etc. (Guo *et al.* 2014; Yu *et al.* 2015; Niu *et al.* 2018; Zhang *et al.* 2018). A large amount of wastewater was produced in the process of production and use, which caused serious environmental pollution and ecological harm (Singh *et al.* 2015; Narvekar *et al.* 2018). In addition, dyes affect the photosynthetic activities of aquatic species due to the color stability, and some of them have high toxicity, carcinogenic, teratogenic and mutagenic effects, and alter gene expression by epigenetic mechanisms (Yao *et al.* 2010; Perullini *et al.* 2014; Ojedokun & Bello 2017; Muthusaravanan *et al.* 2018; Sharavanan *et al.* 2019). Therefore, removal of dyes from wastewater has attracted much attention for decades. Various methods such as adsorption, flocculation, electrochemical, photocatalysis, advanced oxidation processes and biological methods have been used for treatment of dyes in water solution (Park *et al.* 2012; Sattarahmady *et al.* 2013; Konicki *et al.* 2017; Moreira *et al.* 2017; Chen *et al.* 2018; Gu *et al.* 2018; Katheresan *et al.* 2018; Zhao *et al.* 2018).

Adsorption treatment has been recognized as a simple and effective method to remove dyes from aqueous solution, due to its high efficiency, convenience, low cost and easy desorption (Ahmed *et al.* 2020; Navya *et al.* 2020). Many studies have reported the adsorption of dyes on carbon-based materials (Al-Degs *et al.* 2009; Asouhidou *et al.* 2009; Ip *et al.* 2010; Gupta & Khatri 2019; Streit *et al.* 2019; Figueiredo *et al.* 2011). Liu *et al.* reported that ordered mesoporous carbon displayed much stronger adsorption than activated carbon (Liu *et al.* 2009). Gupta & Khatri reported

doi: 10.2166/wst.2020.550

that the specific area and surface polarity conducted fast and efficient adsorptive removal of organic dyes (Gupta & Khatri 2019). Therefore, carbon-based materials with enlarged pore size avoid the size exclusion effect, leading to relatively high adsorption capacity especially for bulky pollutants.

Covalent triazine-based frameworks (CTFs) were first reported in 2008 (Kuhn *et al*. 2008a). They have attracted great attention for energy gas storage and catalytic support materials (Chan-Thaw *et al.* 2010; Li *et al.* 2018; Jena *et al.* 2018), because of the very large specific surface area, homogeneous pore structure, and high chemical and thermal stability (Kuhn *et al.* 2008a, 2008b; Kuhn *et al*. 2009). We reported that a synthesized CTF showed high adsorption affinity, fast adsorption/desorption kinetics, and complete adsorption reversibility for monoaromatic compounds (Liu *et al.* 2012). In addition, CTFs displayed high adsorption affinity for organic pollutants in previous studies (Liu *et al.* 2012, 2013, 2015, 2017; Zhang *et al.* 2011, 2020). These properties make CTFs a promising adsorbent for the removal of organic contaminants in water treatment. However, to the best of our knowledge, little study has reported the adsorption of dyes on CTFs and the adsorption mechanisms and the role of pore distribution were not well understood.

The objective of this work is to explain the adsorption mechanism for three dyes on CTFs and study the roles of CTF pore structure for adsorption. The synthesized CTFs were characterized by XRD, FTIR and N_2 adsorption/desorption isotherms. Pore size distribution and the effect of pH were further performed to understand the mechanisms.

EXPERIMENTAL SECTION

Materials

Methylene blue (MB) and methyl orange (MO) were purchased from Tianjin Institute of Chemical Co., Ltd. Chrysophenine G (CG) was supplied by Tokyo Chemical Industry. 1,4-Dicyanobenzene and 4.4′-biphyldicarbonitrile were purchased from purchased from Aldrich. Chemical structures of MB, MO and CG are presented in Supporting Information (SI) Figure S1.

Preparation of CTFs

Two different CTFs (named CTF-1 and CTF_{DCBP}) were synthesized using monomer 1,4-dicyanobenzene and 4.4′-biphenyldicarbonitrile according to literature method (Kuhn *et al.* 2008a). The details of the synthesis are listed in SI Text S1 and the structures of CTF-1 and CTF_{DCBP} are presented in SI Figure S2.

Characterization of CTFs

X-ray diffraction (XRD) pattern of CTFs was collected from a RigakuD/max-RA powder diffraction-meter using Cu Kα radiation (Rigaku, Japan). Elemental analysis of CTFs was performed in an elemental analyzer of Vario MICRO (Elementar, Germany). Transmission electron microscope (TEM) images of the CTFs were obtained from a JEM-2100 transmission electron microscope. Transmission Fourier transform infrared (FTIR) spectrums of the CTFs were measured using a Nexus 870 spectrometer (Nicolet, USA USA). BET and pore size distribution were obtained on a Micromeritics ASAP 2020 apparatus at −196 °C (Micromeritics Instrument Co., USA).

Adsorption

Adsorption isotherms were conducted by batch adsorption experiment. Briefly, adsorptions (20 mg of CTF-1 and 10 mg of CTF_{DCBP}) were introduced into 40 ml glass vials equipped with polytetrafluoroethylene-lined receiving 40 mL of dyes solution with varied intial concentrations (background solution: 0.02 M NaCl). The samples were mixed using an orbital shaker protected from light at room temperature for 48 h. After filtration, the solute was analyzed using UV–vis spectrometer with detecting wavelengths at 664, 462 and 400 nm for MB, MO and CG, respectively. All adsorption experiments were conducted in duplicate.

Separate sets of experiments were performed to test the effects of pH and ionic strength. In the pH experiments, 10 mg CTF-1 and 40 ml of 50 mg/L MB solutin (80 mg/L MO and 12.5 mg/L CG) with different pH was preadjusted using 0.1 M HCl and NaOH to ensure the desired pH (3–11) at adsorption equilibrium. In the ionic strength experiments, adsorption was performed using background solutions (0.01, 0.02, 0.05, and 0.1 M) NaCl or $CaCl_2$ with 10 mg CTF-1 and 40 ml of 90 mg/L MB solutin (75 mg/L MO and 20 mg/L CG).

Pore size distribution of CTFs

The pore size distribution of the adsorbents before and after adsorption were collected by N_2 adsorption/desorption isotherms. The adsorbents after adsorption filtered with

0.45 μm fiber filter and dried at 40 °C using a vacuum drying oven. Prior to determine pore size distribution, the adsorbents (CTF-1 and CTF_{DCBP}) were activated at 200 °C, and the adsorbents after loading the dyes were activated at 80 °C.

RESULTS AND DISCUSSION

Characterization of CTFs

XRD patterns of the CTFs are displyed in SI Figure S3. The diffraction peaks at 2θ 7.2° and 15.1° for CTF-1, reflecting the crystalline triazine-based organic framework with hexagonal pores (Kuhn *et al.* 2008a). Compared with XRD patterns of the CTF-1, CTF_{DCBP} showed high disordered crystal because of the salt templating effect (Kuhn *et al.* 2009). Nitrogen adsorption/desorption isotherms of CTFs are presented in SI Figure S4. Obviously, typical capillary condensation was observed within a relative pressure range of 0.2–0.9 for adsorbent of CTF_{DCBP}, reflecting the presence of mesoporous. TEM images of CTFs are displayed in SI Figure S5. Similar morphologies are obtained for the CTF-1 and CTF_{DCBP}. CTFs presents a homogeneous structure with microporosity, while the structure of CTF_{DCBP} becomes rough with increasing mesopore size. BET and pore volume of CTFs are listed in Table 1. The BET surface area of the CTF-1 and CTF_{DCBP} were 782.44 and 1,745.45 m^2/g, and the pore volume were 0.4 and 1.42 $cm^3 \cdot g^{-1}$. In addition, micropores were the major pores of CTF-1, while both micropores and mesopores were detected in CTF_{DCBP}. The transmission FTIR spectrum of CTFs is shown in Figure 1. As shown in Figure 1, the strong peaks around 1,352 and 1,507 cm^{-1} are assigned to vibrations of the triazine structure (Bojdys *et al.* 2010).

Table 1 | Specific surface area, and total pore volume adsorbents before and after adsorption of methylene blue (MB), methyl orange (MO) and chrysophenine G (CG). on CTF-1 and CTF_{DCBP}

CTF-1	Specific surface area[a] (m^2/g)	V_t^b (cm^3/g)	CTF_{DCBP}	Specific surface area[a] (m^2/g)	V_t^b (cm^3/g)
Blank	782.0	0.40	Blank	1745.45	1.42
MB	361.35	0.160	MB	602.99	0.476
MO	328.04	0.179	MO	540.77	0.437
CG	642.0	0.316	CG	238.0	0.276

[a]Determined by N_2 adsorption using the Brunauer-Emmett-Teller (BET) method.
[b]Total pore volume, determined at $P/P_0 = 0.976$.

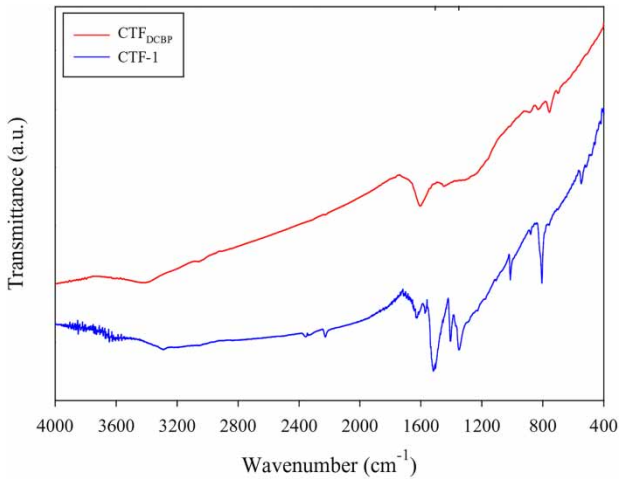

Figure 1 | Transmission Fourier transform infrared (FTIR) spectrum of covalent triazine-based frameworks.

Adsorption isotherms

Adsorption isotherms for three dyes on CTFs are presented in Figure 2. Different trends of the adsorption curves between CTF-1 and CTF_{DCBP} are observed in Figure 2. Adsorption of dyes on the CTF-1 is ordered as follows: MB ≈ MO > CG. The adsorbent-to-solution distribution coefficient (K_d) on CTF-1 was 10^3–10^5 L/kg for MB, 10^3–10^6 L/kg for MO, and 10^2–10^3 L/kg for CG. However, the adsorption on CTF_{DCBP} is ordered as CG > MB ≈ MO. The K_d value on CTF_{DCBP} was 10^4–10^6 L/kg for MB, 10^4–10^6 L/kg for MO, and 10^4–10^6 L/kg for CG. The adsorption data were fitted to the Langmuir and Freundlich model according to Equations (1) and (2):

$$q_e = \frac{q_m b C_e}{1 + bC_e} \quad (1)$$

$$q_e = K_F C_e^{1/n} \quad (2)$$

where q_e (mmol/g) and C_e (mmol/L) are the adsorbed concentration and the aqueous concentration at adsorption equilibrium, q_m(mmol/g) is the adsorption capacity, and b (L/mmol) is the Langmuir affinity coefficient, K_F ($mg^{1-n}\ L^n/g$) is the Freundlich affinity coefficient; n is the Freundlich linearity index. The fitting parameters are summarized in SI Table S2. Adsorption of three dyes to the CTFs can be well described by the Freundlich model with R^2 higher than 0.93. In addtion, the linearity indexes (n) are smaller than 1, suggesting adsorption heterogeneity.

The cavity of CTF is composed of benzene rings and triazine rings that form a large conjugated chain

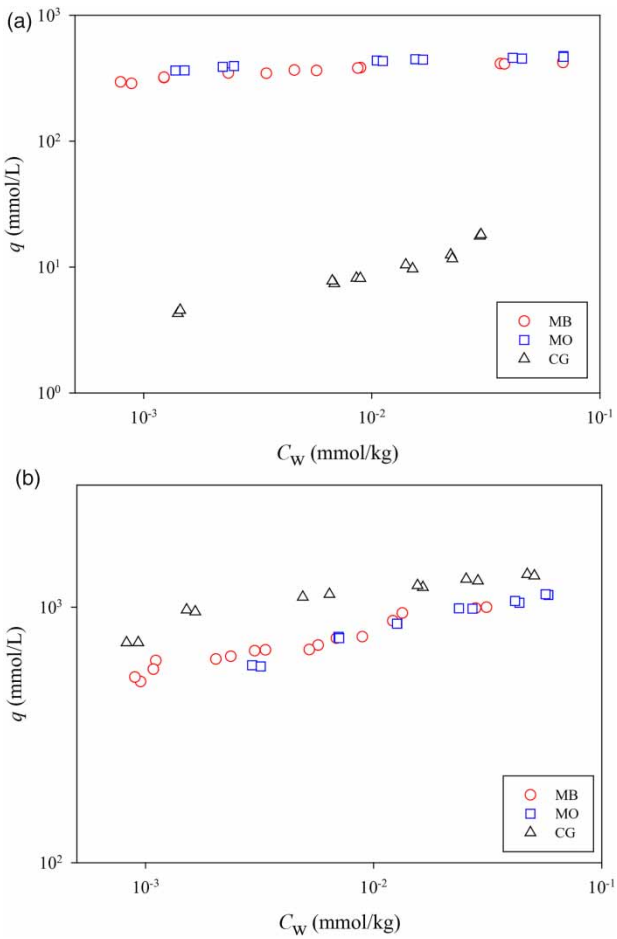

Figure 2 | Adsorption isotherms plotted as solid-phase concentration (q) vs aqueous-phase concentration (C_W) at equilibrium for different dyes on CTF-1 (a) and CTF_{DCBP} (b).

structure, which is rich in π electrons and can be used as π-electron donor (Liu *et al.* 2012). MB as a cationic dye has protonated N atoms. Therefore, cation-π interaction mechanism is generated between protonated N in MB and π-electrons in the surface of CTFs, leading the strong adsorption affinity of MB on CTFs. It is note that adsorption of MO on CTF-1 and CTF_{DCBP} was close to MB, but adsorption mechanism is different. Electrostatic interaction is likely responsible for the strong adsorption of the dye MO. As shown in SI Figure S6, the point of zero charge (PZC) for CTF-1 and CTF_{DCBP} are at pH 7.2 and 8.0. Therefore, the CTFs is positively charged and forming electrostatic interaction with anionic MO. In addtion, the triazine structure has a strong ability to form hydrogen bonds, and hydrogen bonding energy between 1,3,5-triazine and water calculation varied from 3.38 to 22.60 $kJ \cdot mol^{-1}$ as the report (Li *et al.* 2007). Hydrogen bonding interaction between polar functional group and triazine structure further enhanced the adsorption of MO CTFs. Similar results reported that hydrogen bonds formed between MO and the surface of biopolymer chitin and water/1,2-dichloroethane (Longhinotti *et al.* 1998; Rinuy *et al.* 2000).

Unit surface area-based adsorption data are compared in Figure 3 to further explain the adsorption patterns between CTF-1 and CTF_{DCBP}. As shown in Figure 3, adsorption for MB and MO on CTF-1 is higher than on CTF_{DCBP}, particularly at low concentration. The strong adsorption for MB and MO on CTF-1 may be caused by the micropore-filling mechanism. Many previous studies (Nguyen *et al.* 2007; Ji *et al.* 2009; Liu *et al.* 2012; Liu *et al.* 2013) have reported this mechansiam. Such as Nguyen *et al.* (Nguyen *et al.* 2007) reported that micropore-filling mechanism enhanced aromatic hydrocarbons adsorption on carbonaceous adsorbents. This agrees well with the pore volume results (see SI Table S1). However, adsorption for CG on CTF-1 is dramatically suppressed by the size exclusion effect due to its large molecules. CTT_{DCBP} displayed higher normalized adsorption than CTF-1 for CG in Figure 3. This attributed to the larger mesopore volume of CTF_{DCBP}, which effectively avoids the size exclusion effect. The importance of pore structure is further discussed in pore size distribution (see below).

Pore size distribution of CTFs

Pore size distribution of CTFs before and after dyes adsorption are compared in Figure 4 and Table 1 to illustrate the impact of adsorbent pore size and adsorbate molecular size. For CTF-1 in Table 1, the total pore volume of CTF-1 decreased from 0.40 cm^3/g to 0.160, 0.179 and 0.316 cm^3/g after adsorption of MB, MO and CG. The slightly change of total pore volume for CG is attribute to large size CG, leading to only adsorption on the external surface of CTF-1 because of the size exclusion effect. However, for CTF_{DCBP} in Figure 4(b), after adsorption of CG most pore diameters around 2 to 4 nm were shifted significantly and pore volume after adsorption of CG was reduced form 1.42 cm^3/g to 0.276 cm^3/g. The strong adsorption for CG on CTF_{DCBP} caused by mesorpore-filling mechanism due to size of the CG (size of CG 2.98 nm displayed in Figure S2) matched with the pore width of CTF_{DCBP}. It is note that the total pore volume MB, MO on CTF_{DCBP} also decreased from 1.42 cm^3/g to 0.476 and 0.437. This indicated that the adsorption sites outside or inside the pores of CTF_{DCBP} were occupied efficiently by

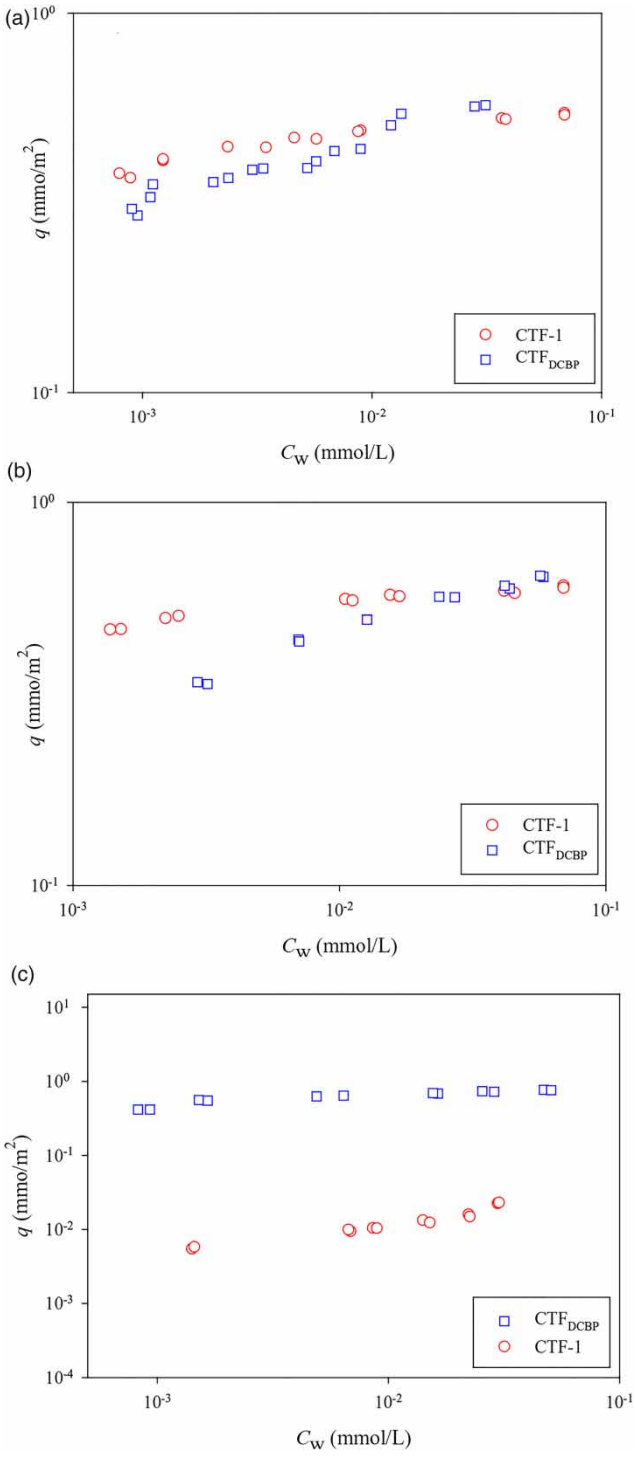

Figure 3 | Adsorption isotherms of antibiotics plotted as surface area-normalized solid-phase concentration (q) vs aqueous-phase concentration (C_w) at adsorption equilibrium on CTF-1 and CTF_{DCBP}. (a) Methylene blue (MB), (b) methyl orange (MO), (c) Chrysophenine G (CG).

MB and MO, which was attributed to the adsorption mechanisms (cation-π, electrostatic interaction and hydrogen bonding) mentioned above.

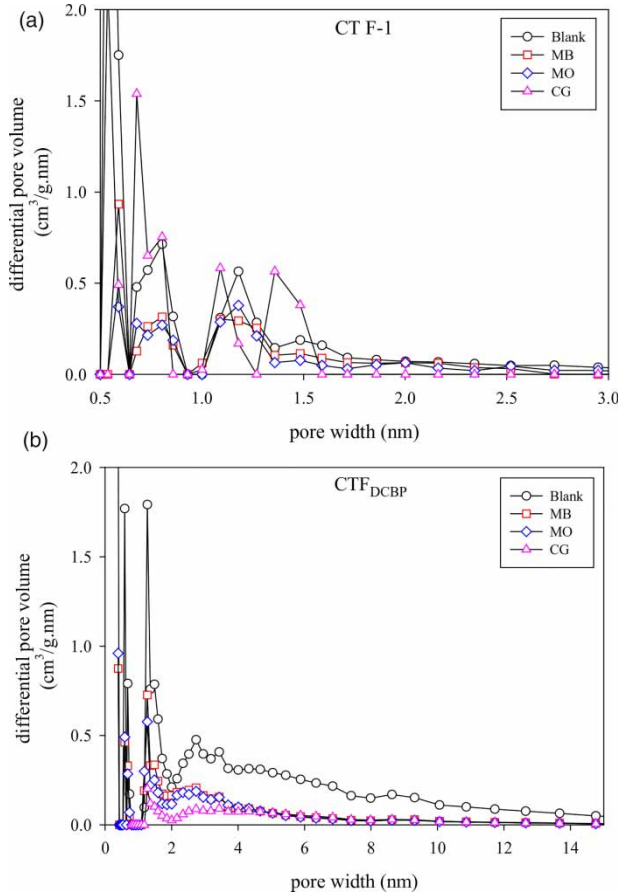

Figure 4 | Pore size distributions of adsorbents before and after adsorption of different adsorbates: methylene blue (MB), methyl orange (MO) and chrysophenine G (CG). (a) CTF-1. (b) CTF_{DCBP}.

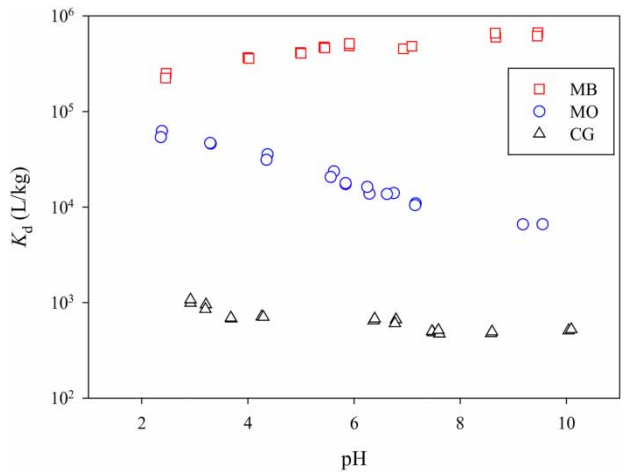

Figure 5 | Changes of adsorbent-to-solution distribution coefficients (K_d) with pH at single point concentrations for adsorption of methylene blue (MB), methyl orange (MO) and chrysophenine G (CG) on CTF-1.

Effects of pH and ionic strength

The effects of pH for three dyes on CTF-1 (CTF_{DCBP} were not studied due to the similar pzc to CTF-1, only difference in pore structure) are presented in Figure 5. As shown in Figure 5, the K_d value increased gradually with the increasing pH for MB. MO and CG decreasd with the increasing pH, suggesting the same adsorptive

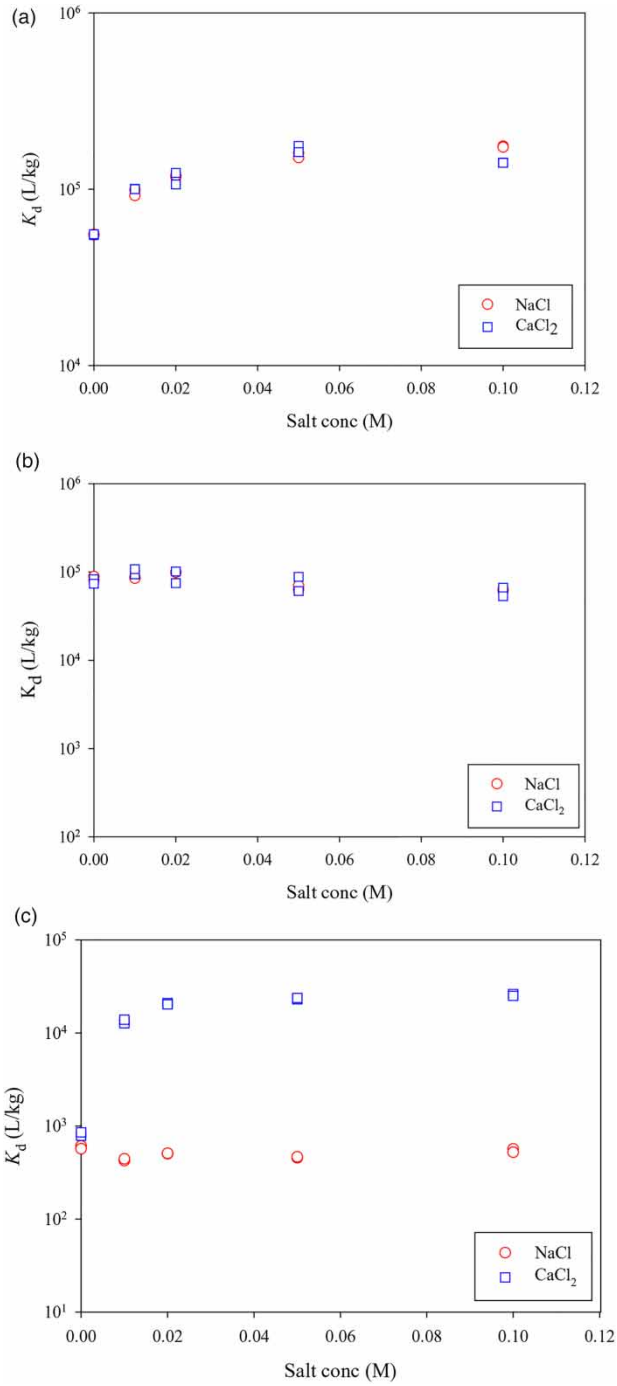

Figure 6 | Effect of ionic strength (NaCl, $CaCl_2$) on adsorption coefficient (K_d) for single-point adsorption of dyes on CTF-1. (a) Methylene blue (MB). (b) Methyl orange (MO). (c) Chrysophenine G (CG).

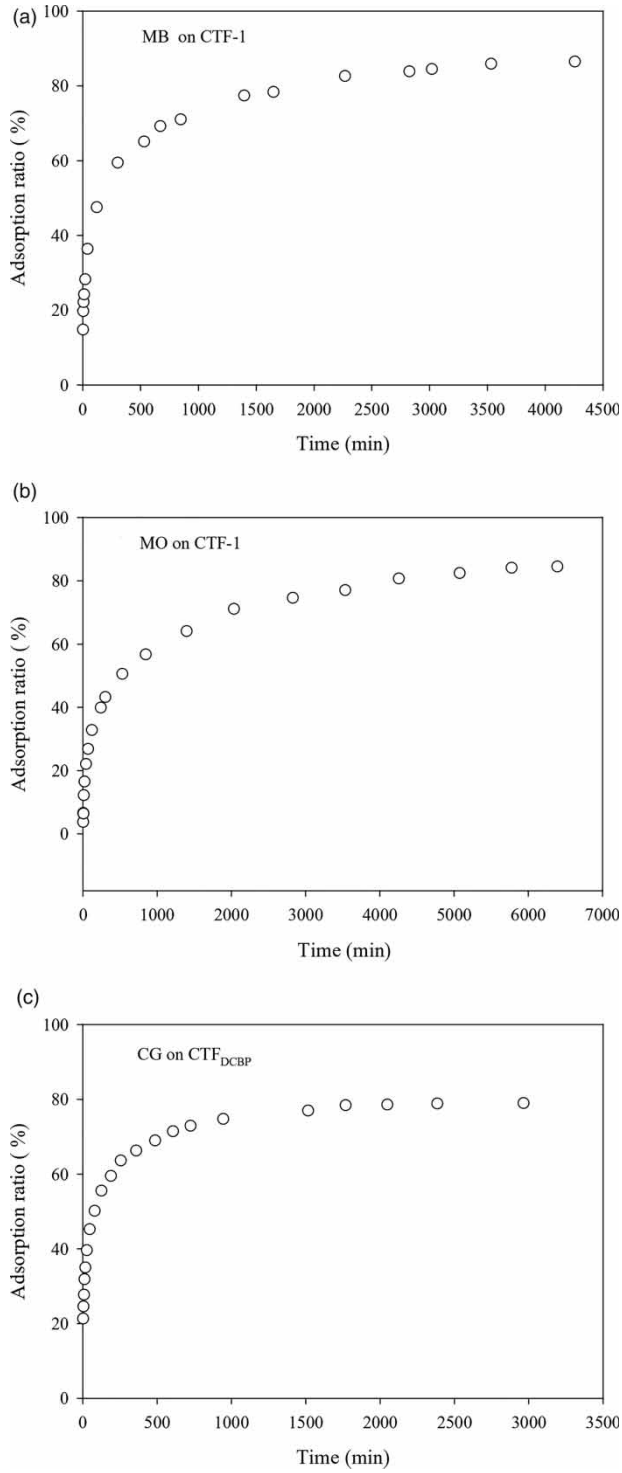

Figure 7 | Adsorption kinetics of dyes on CTFs. Methylene blue on CTF-1 (a), Methyl orange (MO) on CTF-1 (b), and Chrysophenine G (CG) on CTF_{DCBP} (c).

Table 2 | Fitting parameters for adsorption kinetics by pseudo-first-order and pseudo-second-order models

		Pseudo-first-order kinetic model			Pseudo-second-order kinetic model		
Dye/adsorbent	q_{exp}/mmol·kg^{-1}	k_1/1·s^{-1}	q_{cal}/mmol·kg^{-1}	R^2	k_2/kg·(mmol^{-1}·s^{-1}	q_{cal}/mmol·kg^{-1}	R^2
MB/CTF-1	577.90	2.21×10^{-4}	353.29	0.972	1.88×10^{-6}	581.39	0.997
MO/CTF-1	644.75	1.41×10^{-4}	497.40	0.959	7.31×10^{-6}	648.93	0.997
CG/CTF$_{DCBP}$	938.14	4.54×10^{-4}	468.82	0.972	8.40×10^{-5}	946.07	0.999

interaction with CTF-1. CTF-1 is deprotonated and negatively charged with the increasing pH as the pzc around pH 7.2 (see SI Figure S6). Electrostatic interaction between cationic dye MB and CTF-1 gradually strengthened. However, the adsorption affinity could be suppressed when the pH continue increasing, because electrostatic repulsion was enhanced between CTF-1 and negatively charged MO and CG. In addtion, adsorption decreased slightly at pH range 7.2–10, indicating that higher pH favored hydrogen bonding interaction with the deprotonated triazine structure.

The effects of ionic strength for dyes on CTF-1 are listed in Figure 6. Clearly, ionic strength promoted MB adsorption on CTF-1. Salting-out effect is responsible for the increasing adsorption coefficient for MB (Grover & Ryall 2005). Similar result has been report in previous studies (Fontecha-Cámara *et al.* 2007; Eren & Afsin 2008). The adsorption of MO and CG decreased with the increasing ionic strength. MO and CG as anionic dyes, the electrostatic screening of the surface charge gradually enhanced with the increasing counterion species, leading to the lower adsorption coefficient. However, Ca^{2+} promoted the adsorption of CG on CTF-1, which may be caused by coordination or complexation between Ca^{2+} and CG.

Adsorption kinetics

Adsorption kinetics of MB and MO on CTF-1 and adsorption kinetics of CG on CTF$_{DCBP}$ are presented in Figure 7. As show in Figure 7, small molecular dyes MB and MO adsorption on CTF-1 reached equilibrium within 3,500 and 5,000 min separately. Of note, adsorption equilibrium for CG on CTF$_{DCBP}$ achieved equilibrium within 200 min. CTF-1 has narrow pore size distribution, and the dye molecules are not easy to diffuse into the interior, leading to relatively slow kinetics. The rapid kinetics for CTF$_{DCBP}$ correlated closely with the shaped, open and wide pore size distribution, which is consistent with the results of adsorbent pore size distribution.

In order to explain the mass transfer process during the dyes' adsorption, pseudo-first-order and pseudo-second-order kinetic models were applied. As the following equation:

$$\log(q_e - q_t) = \log(q_e) - \frac{k_1 t}{2.303} \tag{3}$$

$$\frac{t}{q_t} = \frac{1}{k_2 q_e^2} - \frac{t}{q_e} \tag{4}$$

where q_e is the equilibrium adsorbed concentration, q_t is the adsorbed concentration at time t, k_1 and k_2 are the pseudo-first order rate constant and the pseudo-second order rate constant, respectively.

Simulation results of dyes adsorption on CTFs based on the pseudo-first-order kinetics and pseudo-second-order kinetics are presented in SI Figure S7, and the fitting parameters are listed in Table 2. As shown in SI Figure S7(b), the plot of t/q_t versus t presenteded a linear relation with a higher R^2 (0.997), suggesting that pseudo-second-order kinetic model could well depict the dyes' adsorption process to CTFs. In addition, the q_{exp} data (obtained from experimental data) are approximately identical to the q_{cal} data (calculated from the pseudo-second-order model) in Table 2, which further confirmed that the dyes' adsorption process on CTFs obeyed the pseudo-second-order kinetics model.

CONCLUSIONS

In this study, two different covalent triazine-based frameworks were synthesized and their adsorption for three dyes was systematically investigated. Characterization results indicated that the CTFs were successfully synthesized with a homogeneous and regular-shaped structure. Adsorption results demonstrated that the selected three dyes have strong adsorption on CTFs adsorbents because of cation–π, electrostatic interaction and hydrogen bonding interaction. Pore size distribution of CTFs is an important factor for adsorption particularly for bulky dyes CG. Acidic conditions are favorable for the adsorption of MB, while alkaline conditions are favorable for the adsorption of MO and CG. The

results in this study indicate that CTFs are promising adsorbents for adsorptive removal of dyes in aqueous solution

ACKNOWLEDGEMENTS

This work was supported by Scientific Research Project of Nanjing Xiaozhuang University (2017NXY46), Excellent Science and Technology Innovation Group of Jiangsu Province, Innovative Practice of Environmental Engineering Subject based on New Engineering Construction.

DATA AVAILABILITY STATEMENT

All relevant data are included in the paper or its Supplementary Information.

REFERENCES

Ahmed, D. N., Naji, L. A., Faisal, A. A. H., Al-Ansari, N. & Naushad, M. 2020 Waste foundry sand/MgFe-layered double hydroxides composite material for efficient removal of Congo Red dye from aqueous solution. *Scientific Reports* **10**, 2042.

Al-Degs, Y. S., Khraisheh, M. A. M., Allen, S. J. & Ahmad, M. N. 2009 Adsorption characteristics of reactive dyes in columns of activated carbon. *Journal of Hazardous Materials* **165**, 944–949.

Asouhidou, D. D., Triantafyllidis, K. S., Lazaridis, N. K., Matis, K. A., Kim, S. S. & Pinnavaia, T. J. 2009 Sorption of reactive dyes from aqueous solutions by ordered hexagonal and disordered mesoporous carbons. *Microporous and Mesoporous Materials* **117**, 257–267.

Bojdys, M. J., Jeromenok, J., Thomas, A. & Antonietti, M. 2010 Rational extension of the family of layered, covalent, triazine-based frameworks with regular porosity. *Advanced Materials* **22**, 2202–2205.

Chan-Thaw, C. E., Villa, A., Katekomol, P., Su, D., Thomas, A. & Prati, L. 2010 Covalent triazine framework as catalytic support for liquid phase reaction. *Nano Letters* **10**, 537–541.

Chen, L., Cai, T., Cheng, C., Xiong, Z. & Ding, D. 2018 Degradation of acetamiprid in UV/H_2O_2 and UV/persulfate systems: a comparative study. *Chemical Engineering Journal* **351**, 1137–1146.

Eren, E. & Afsin, B. 2008 Investigation of a basic dye adsorption from aqueous solution onto raw and pre-treated bentonite surfaces. *Dyes and Pigments* **76**, 220–225.

Figueiredo, J. L., Sousa, J. P. S., Orge, C. A., Pereira, M. F. R. & Órfão, J. J. M. 2011 Adsorption of dyes on carbon xerogels and templated carbons: influence of surface chemistry. *Adsorption* **17**, 431–441.

Fontecha-Cámara, M. A., López-Ramón, M. V., Álvarez-Merino, M. A. & Moreno-Castilla, C. 2007 Effect of surface chemistry, solution pH, and ionic strength on the removal of herbicides diuron and amitrole from water by an activated carbon fiber. *Langmuir* **23**, 1242–1247.

Grover, P. K. & Ryall, R. L. 2005 Critical appraisal of salting-out and its implications for chemical and biological sciences. *Chemical Reviews* **105**, 1–10.

Gu, M., Yin, Q., Wang, Z., He, K. & Wu, G. 2018 Color and nitrogen removal from synthetic dye wastewater in an integrated mesophilic hydrolysis/acidification and multiple anoxic/aerobic process. *Chemosphere* **212**, 881–889.

Guo, J. Z., Li, B., Liu, L. & Lv, K. 2014 Removal of methylene blue from aqueous solutions by chemically modified bamboo. *Chemosphere* **111**, 225–231.

Gupta, K. & Khatri, O. P. 2019 Fast and efficient adsorptive removal of organic dyes and active pharmaceutical ingredient by microporous carbon: effect of molecular size and charge. *Chemical Engineering Journal* **378**, 122218.

Ip, A. W. M., Barford, J. P. & McKay, G. 2010 A comparative study on the kinetics and mechanisms of removal of Reactive Black 5 by adsorption onto activated carbons and bone char. *Chemical Engineering Journal* **157**, 434–442.

Jena, H. S., Krishnaraj, C., Wang, G., Leus, K., Schmidt, J., Chaoui, N. & Van Der Voort, P. 2018 Acetylacetone covalent triazine framework: an efficient carbon capture and storage material and a highly stable heterogeneous catalyst. *Chemistry of Materials* **30**, 4102–4111.

Ji, L., Chen, W., Duan, L. & Zhu, D. 2009 Mechanisms for strong adsorption of tetracycline to carbon nanotubes: a comparative study using activated carbon and graphite as adsorbents. *Environmental Science & Technology* **43**, 2322–2327.

Katheresan, V., Kansedo, J. & Lau, S. Y. 2018 Efficiency of various recent wastewater dye removal methods: a review. *Journal of Environmental Chemical Engineering* **6**, 4676–4697.

Konicki, W., Aleksandrzak, M., Moszyński, D. & Mijowska, E. 2017 Adsorption of anionic azo-dyes from aqueous solutions onto graphene oxide: equilibrium, kinetic and thermodynamic studies. *Journal of Colloid and Interface Science* **496**, 188–200.

Kuhn, P., Antonietti, M. & Thomas, A. 2008a Porous, covalent triazine-based frameworks prepared by ionothermal synthesis. *Angewandte Chemie International Edition* **47**, 3450–3453.

Kuhn, P., Krüger, K., Thomas, A. & Antonietti, M. 2008b Everything is surface: tunable polymer organic frameworks with ultrahigh dye sorption capacity. *Chemical Communications (Cambridge, England)* **44**, 5815–5817.

Kuhn, P., Thomas, A. & Antonietti, M. 2009 Toward tailorable porous organic polymer networks: a high-temperature dynamic polymerization scheme based on aromatic nitriles. *Macromolecules* **42**, 319–326.

Li, Q., Hu, J. D. & Zhao, K. Q. 2007 DFT study of Hydrogen-bonded 1,3,5-triazine-water complexes. *Chinese Journal of Chemistry* **25**, 1078–1081.

Li, Y., Zheng, S., Liu, X., Li, P., Sun, L., Yang, R., Wang, S., Wu, Z.-S., Bao, X. & Deng, W.-Q. 2018 Conductive microporous covalent triazine-based framework for high-performance electrochemical capacitive energy storage. *Angewandte Chemie (International ed. in English* **57**, 7992–7996.

Liu, F., Wang, J., Li, L., Shao, Y., Xu, Z. & Zheng, S. 2009 Adsorption of direct yellow 12 onto ordered mesoporous

carbon and activated carbon. *Journal of Chemical & Engineering Data* **54**, 3043–3050.

Liu, J., Zong, E., Fu, H., Zheng, S., Xu, Z. & Zhu, D. 2012 Adsorption of aromatic compounds on porous covalent triazine-based framework. *Journal of Colloid and Interface Science* **372**, 99–107.

Liu, J., Chen, H., Zheng, S. & Xu, Z. 2013 Adsorption of 4,4′-(Propane-2,2-diyl)diphenol from aqueous solution by a covalent triazine-based framework. *Journal of Chemical & Engineering Data* **58**, 3557–3562.

Liu, J., Cao, J., Chen, H. & Zhou, D. 2015 Adsorptive removal of humic acid from aqueous solution by micro- and mesoporous covalent triazine-based framework. *Colloids and Surfaces A: Physicochemical and Engineering Aspects* **481**, 276–282.

Liu, J., Zhou, D., Xu, Z. & Zheng, S. 2017 Adsorptive removal of pharmaceutical antibiotics from aqueous solution by porous covalent triazine frameworks. *Environmental Pollution* **226**, 379–384.

Longhinotti, E., Pozza, F., Furlan, L., Sanchez, M. D. N. D. M., Klug, M., Laranjeira, M. & Fávere, V. T. 1998 Adsorption of anionic dyes on the biopolymer chitin. *Journal of the Brazilian Chemical Society* **9**, 435–440.

Moreira, F. C., Boaventura, R. A. R., Brillas, E. & Vilar, V. J. P. 2017 Electrochemical advanced oxidation processes: a review on their application to synthetic and real wastewaters. *Applied Catalysis B: Environmental* **202**, 217–261.

Muthusaravanan, S., Sivarajasekar, N., Vivek, J. S., Paramasivan, T., Naushad, M., Prakashmaran, J., Gayathri, V. & Al-Duaij, O. K. 2018 Phytoremediation of heavy metals: mechanisms, methods and enhancements. *Environmental Chemistry Letters* **16**, 1339–1359.

Narvekar, A. A., Fernandes, J. B. & Tilve, S. G. 2018 Adsorption behavior of methylene blue on glycerol based carbon materials. *Journal of Environmental Chemical Engineering* **6**, 1714–1725.

Navya, A., Shellakkutti, N., Sivamani, S., Vasu, G., Sivarajasekar, N. & Hosseini-Bandegharaei, A. 2020 Preparation and characterization of cassava stem biochar for mixed reactive dyes removal from simulated effluent. *Desalination and Water Treatment* **189**, 440–451.

Nguyen, T. H., Cho, H.-H., Poster, D. L. & Ball, W. P. 2007 Evidence for a pore-filling mechanism in the adsorption of aromatic hydrocarbons to a natural wood char. *Environmental Science & Technology* **41**, 1212–1217.

Niu, T., Zhou, J., Zhang, C. & Li, S. 2018 Fast removal of methylene blue from aqueous solution using coal-based activated carbon. *RSC Advances* **8**, 26978–26986.

Ojedokun, A. T. & Bello, O. S. 2017 Kinetic modeling of liquid-phase adsorption of Congo red dye using guava leaf-based activated carbon. *Applied Water Science* **7**, 1965–1977.

Park, J. H., Ko, K. C., Kim, E., Park, N., Ko, J. H., Ryu, D. H., Ahn, T. K., Lee, J. Y. & Son, S. U. 2012 Photocatalysis by phenothiazine dyes: visible-light-driven oxidative coupling of primary amines at ambient temperature. *Organic Letters* **14**, 5502–5505.

Perullini, M., Jobbágy, M., Japas, M. L. & Bilmes, S. A. 2014 New method for the simultaneous determination of diffusion and adsorption of dyes in silica hydrogels. *Journal of Colloid and Interface Science* **425**, 91–95.

Rinuy, J., Piron, A., Brevet, P. F. o., Blanchard-Desce, M. & Girault, H. H. 2000 Intramolecular electron density redistribution upon hydrogen bond formation in the anion methyl orange at the water/1, 2-Dichloroethane interface probed by phase interference second harmonic generation. *Chemistry – A European Journal* **6**, 3434–3441.

Sattarahmady, N., Heli, H. & Moradi, S. E. 2013 Cobalt hexacyanoferrate/graphene nanocomposite – application for the electrocatalytic oxidation and amperometric determination of captopril. *Sensors and Actuators B: Chemical* **177**, 1098–1106.

Sharavanan, V. J., Sivaramakrishnan, M., Sivarajasekar, N., Senthilrani, N., Kothandan, R., Dhakal, N., Sivamani, S., Show, P. L., Awual, M. R. & Naushad, M. 2019 Pollutants inducing epigenetic changes and diseases. *Environmental Chemistry Letters* **18**, 325–343.

Singh, R. L., Singh, P. K. & Singh, R. P. 2015 Enzymatic decolorization and degradation of azo dyes – a review. *International Biodeterioration & Biodegradation* **104**, 21–31.

Streit, A. F. M., Côrtes, L. N., Druzian, S. P., Godinho, M., Collazzo, G. C., Perondi, D. & Dotto, G. L. 2019 Development of high quality activated carbon from biological sludge and its application for dyes removal from aqueous solutions. *Science of The Total Environment* **660**, 277–287.

Yao, Y., Xu, F., Chen, M., Xu, Z. & Zhu, Z. 2010 Adsorption behavior of methylene blue on carbon nanotubes. *Bioresource Technology* **101**, 3040–3046.

Yu, J. X., Cai, X. L., Feng, L. Y., Xiong, W. L., Zhu, J., Xu, Y. L., Zhang, Y. F. & Chi, R. A. 2015 Synergistic and competitive adsorption of cationic and anionic dyes on polymer modified yeast prepared at room temperature. *Journal of the Taiwan Institute of Chemical Engineers* **57**, 98–103.

Zhang, W., Liang, F., Li, C., Qiu, L. G., Yuan, Y. P., Peng, F. M., Jiang, X., Xie, A. J., Shen, Y. H. & Zhu, J. F. 2011 Microwave-enhanced synthesis of magnetic porous covalent triazine-based framework composites for fast separation of organic dye from aqueous solution. *Journal of Hazardous Materials* **186**, 984–990.

Zhang, Y., Li, J., Zhao, J., Zhang, Y. F. & Fan, J. 2018 Utilization of modified *Dioscorea opposita Thunb.* as a novel biosorbent for the adsorption of indigo carmine in aqueous solutions. *RSC Advances* **8**, 30040–30048.

Zhang, N., Ishag, A., Li, Y., Wang, H., Guo, H., Mei, P., Meng, Q. & Sun, Y. 2020 Recent investigations and progress in environmental remediation by using covalent organic framework-based adsorption method: a review. *Journal of Cleaner Production* **277**, 123360.

Zhao, C., Zheng, H., Sun, Y., Zhang, S., Liang, J., Liu, Y. & An, Y. 2018 Evaluation of a novel dextran-based flocculant on treatment of dye wastewater: effect of kaolin particles. *Science of the Total Environment* **640–641**, 243–254.

First received 27 August 2020; accepted in revised form 2 November 2020. Available online 16 November 2020